



Chemical and isotopic characteristics and origins of thermal springs in the Jiangcang Basin, China

Zhenxing Wang^{1,2} · Xiangquan Li^{1,2}

Received: 17 September 2020 / Accepted: 23 December 2020 / Published online: 15 February 2021
© Saudi Society for Geosciences 2021

Abstract

Thermal springs in the Jiangcang Basin occur in a typical geothermal zone along the northeastern edge of the Qinghai-Tibet Plateau in the northern Qilian orogenic belt. The thermal spring water (TSW) in this region can be divided into three groups on the basis of temperature and salinity, but the origin and recharge-discharge mechanism of the geothermal fluid remain unclear. The chemical and isotopic characteristics of these thermal springs were studied, and the genesis of the thermal system hosted by deep-seated faults was assessed. The results indicate that the springs in this region are of meteoric origin and heated via deep circulation through well-developed faults. The TSW in the Datong River washland and in the southern part of the basin are derived from carbonate rocks recharged from Datong Mountain, whereas the TSW in the northern part of the basin originates from silicates recharged from Tuolai Mountain. Differences in the circulation depth, flow pathway, residence time, and mixing relationship with cold water lead to different TWS characteristics. The results are used to establish a conceptual model of the origins and circulation of the Jiangcang thermal springs. These findings provide a geological and scientific basis for the development and use of geothermal resources in the northeastern Qinghai-Tibet Plateau.

Keywords Thermal springs · Hydrochemistry · Isotopes · Reservoir temperature · Jiangcang Basin

Introduction

Geothermal resources have attracted considerable attention in recent years as a clean energy source (e.g., Wang et al. 2000; Vonsée et al. 2019). Several studies have addressed the chemical and isotopic composition of thermal springs to better understand the factors that influence their hydrogeochemical characteristics and origins (e.g., Vonsée et al. 2019; Truesdell and Hulston 2017; Giggenbach et al. 1983; Giggenbach 1988; Caron et al. 2008; Chatterjee et al. 2017; Sabria et al. 2019). The Qinghai-Tibet Plateau and its

surroundings are rich in geothermal resources with high water volumes and temperatures. Previous studies on the geothermal systems in this area have investigated springs in the Tibetan Plateau (Tan et al. 2014), Yanjing, Tibet (Qi et al. 2018), Jifei hot spring in Yunnan (Liu et al. 2015), Lanping-Simao Basin (Bo et al. 2015), Xining Basin (Li et al. 2007; Tan et al. 2012), and southern Gaoligong Mountains (Li et al. 2014). These studies mainly addressed the characteristics of the recharge waters, reservoir temperature, circulation depth, residence time, and water mixing processes.

The concentration of major ions and trace elements in groundwater from different aquifers can be used to investigate their origins and mixing (Gibson and Hinman 2013; Bo et al. 2015; Qi et al. 2018). Hydrogeochemical and isotopic data are also indicative structural elements of geothermal systems (Favara et al. 2001; Liu et al. 2015). Stable isotopes have been extensively used as tracers for hydrological cycles (Liu et al. 2015; Fu et al. 2018). In particular, the $^{87}\text{Sr}/^{86}\text{Sr}$ ratio can be used to trace elemental resources and groundwater flowing pathways (Wang et al. 2009; Bo et al. 2015), and $\delta^{18}\text{O}$ and $\delta^{34}\text{S}$ are widely used to identify the source of sulfates in groundwater and the openness of a storage environment (Li et al. 2014; Jonathan et al. 2010).

Responsible Editor: Broder J. Merkel

✉ Xiangquan Li
ihexql1966@163.com

¹ Institute of Hydrogeology and Environmental Geology, Chinese Academy of Geological Sciences, Shijiazhuang 050061, Hebei, China

² Key Laboratory of Groundwater Sciences and Engineering, Ministry of Natural Resources, Shijiazhuang 050061, Hebei, China

The thermal spring water (TSW) in the Jiangcang Basin can be divided into three groups according to temperature and salinity. Preliminary geological and hydrochemical investigations have been carried out in the Jiangcang Basin since the 1970s including studies of the hydrogeological structure and groundwater type (Regional Hydrogeological Survey Report 1978, 1987). However, research is scarce on the thermal springs in this area, including the Muliqugu, Datonghe, and Zemoyesang springs, and the origin and recharge-discharge mechanism of the geothermal fluid remain unclear.

In this study, a detailed geochemical investigation was conducted on the thermal water in the Jiangcang Basin. The ionic and isotope characteristics of the thermal waters and rocks were analyzed to (i) characterize the geochemical properties of the hydrothermal waters; (ii) investigate the origin and formation mechanism of the TSW; and (iii) understand their circulation pathway. The results provide a geological and scientific basis for the development and use of geothermal resources in the northeastern Qinghai-Tibet Plateau.

Geological setting

The thermal springs in the Jiangcang Basin occur in a typical geothermal zone along the northeastern edge of the Qinghai-Tibet Plateau in the northern Qilian orogenic belt. The Jiangcang Basin belongs to the middle Qilian orogenic belt, which is a NW-SE oceanic fracture belt between the northern and southern Qilian blocks (Fig. 1). The zone is composed of subduction accretion complexes including Neoproterozoic to early Paleozoic metamorphic rocks and post-sedimentary cover sequences of Carboniferous, Permian, Triassic, Jurassic, and Quaternary ages (Wei et al. 2018).

The major faults in this region are predominantly reverse faults. The deep F_2 fault represents the boundary between the middle Qilian uplift belt (I_2) and south Qilian geosynclinal belt (I_3), and the deep F_{11} fault marks the boundary between the middle Qilian uplift belt (I_2) and north Qilian geosynclinal belt (I_1) (Song et al. 2013; Chen et al. 2019) (Fig. 1a). The rocks are deformed, and breccia and scratches are observable along the faults. The F_9 and F_{10} faults north of the Datong River are distributed NW-SE, which is consistent with the regional tectonic line direction. The F_4 – F_6 faults south of the Datong River are distributed in the W-E direction (Fig. 1b). The fault displacements in the basin stretch over hundreds of meters.

The sloping plain in the Jiangcang Basin is composed of a gravel layer of glacial and fluvio-glacial deposits that contain boulders. The hills in the center of the basin are composed of plagiogneiss, marble, sandstone, mudstone, and coal. Limestone, dolomite, and sandstone are distributed in the southern part of the basin, and sandstone, mudstone, and coal are distributed in the northern part of the basin (Fig. 1).

The altitude of the study area ranges from 3700 to 4800 m. This region is characterized by an alpine climate with an annual average precipitation of more than 500 mm and temperature of -2.8 °C.

Hydrogeology

Permafrost is distributed in the region as an aquifuge. The groundwater can be divided into supraperafrost and infraperafrost waters, which are located in both the active layer above the permafrost and confined below the permafrost. The thermal springs are another type of groundwater with deeper circulation depths and longer flow pathways. The recharge runoff and discharge processes of the geothermal springs are controlled by faults.

The supraperafrost aquifer in the Jiangcang Basin is lithologically formed by the accumulation of Quaternary glacial moraine, sand, and gravel. The aquifer thickness, which is controlled by the seasonal melting depth, is generally within 3 m. The supraperafrost water takes the permafrost as the lower confining bed and drains in the form of descending springs in the gullies. The direction of movement varies with the terrain and eventually drains into the river.

Infraperafrost water is distributed in the rock strata below the frozen soil layer in the Jiangcang Basin. The aquifer is mainly composed of sandstone, limestone, marble, and some loose Quaternary strata. The infraperafrost water takes the permafrost as the upper confining bed and discharges in the form of fault springs.

The thermal springs infiltrate the fault zone of the mountainous area. Groundwater flows along the structural channel and in the exposed basin within the deep and large tectonic complex.

Thermal spring water in the north of the basin (TSW-N) —Muliqugu spring

The vent of the Muliqugu spring (sampling sites H1–H3) is exposed at the top of a 50-m-high travertine hill, which occurs at the junction of a major NWW-trending compressive fault (the Datong River north bank fault) and a NNE-trending compressive torsional fracture. The discharge rate of the spring groups is higher than 50 L/s, and the water temperature is 35.6–36.6 °C.

Thermal spring water in the Datong river washland (TSW-D) —Datonghe spring

The Datonghe spring (sampling site H4) is located on the floodplain of the Datong River. The spring water is exposed along a major NWW-trending compressive fault (the Datong River fault). The discharge rate of the spring is approximately 1.5 L/s. The spring mouth is flooded by the river during flooding periods, and the spring water temperature is 8.9 °C.

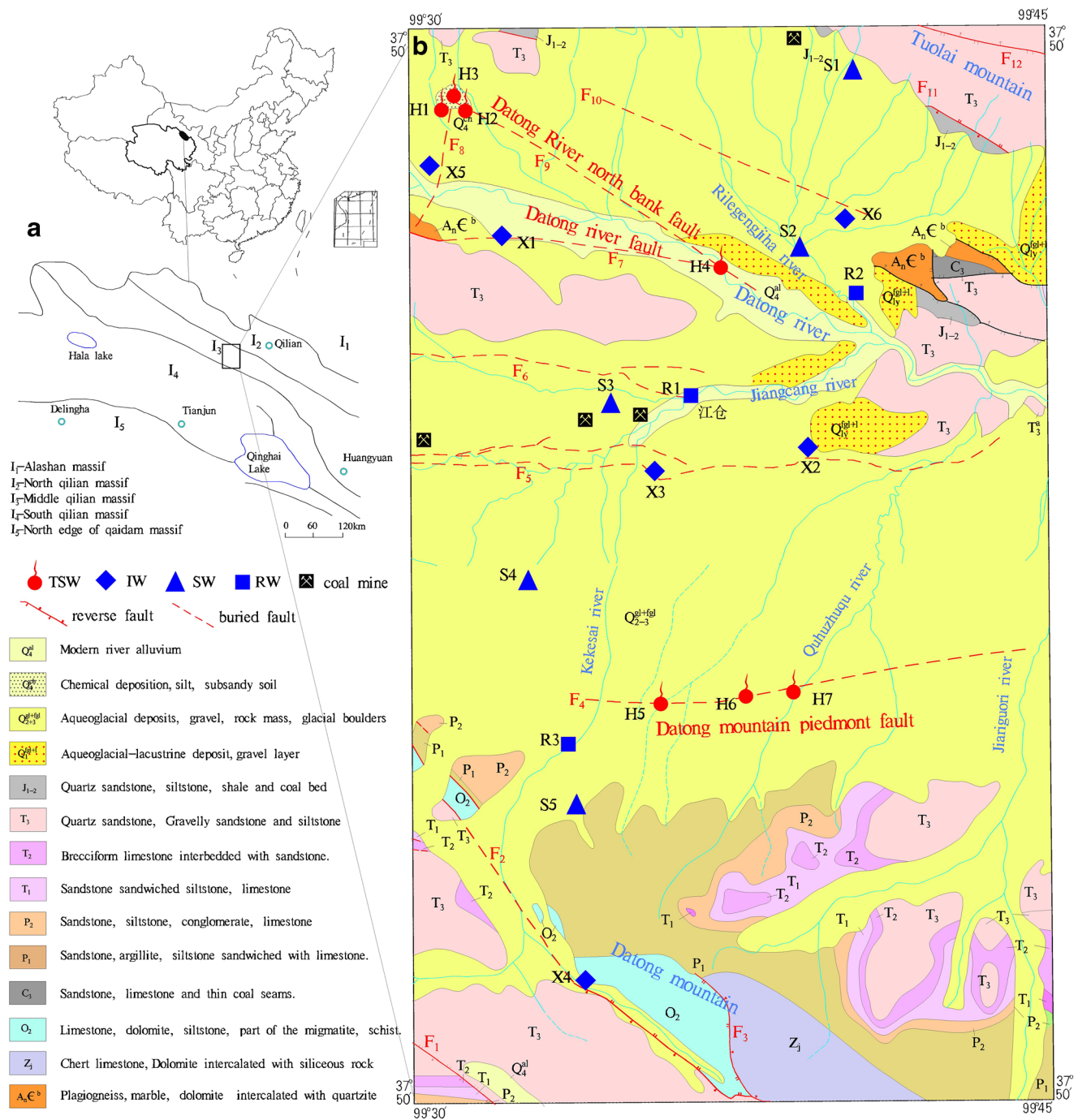


Fig. 1 Study area location and sampling sites. **a** Regional tectonic outline. **b** Jiangcang Basin geologic map

Thermal spring water in the south of the basin (TSW-S: H5–H7)—Zemoyesang spring (H5)

The springs in this area (sampling sites H5–H7) are exposed along a W-E compressive fault (Datong Mountain piedmont fault, F₄). The Zemoyesang spring (H5) is the largest among these with travertine 11 m above the ground. The spring water flows over the top of the travertine with a discharge rate of 2.9 L/s and water temperature of 24 °C.

Materials and methods

Sample preparation

Seven thermal spring water (TSW), six suprapernmafrost spring water (SSW), five infrapermafrost water (IW), and three river water (RW) samples were collected. The sampling sites are shown in Fig. 1. The water samples were first filtered through 0.45-µm membrane filters according to the test requirements. The

samples designated for major ion analysis were then poured into 1.5-L polyethylene bottles without further treatment. The samples for trace element analysis were acidified to pH < 2 by adding nitric acid and contained within 500-mL polyethylene bottles. The samples for stable isotope analysis ($\delta^{18}\text{O}$ and δD) were sealed in 500-mL glass bottles with airtight caps. Nine additional samples were stored individually in 5-L buckets for $\delta^{18}\text{O}_{\text{SO}_4}$ and $\delta^{34}\text{S}_{\text{SO}_4}$ analyses. The samples were maintained below 4 °C and sent to the laboratory within 3 days. Samples were also collected at the bottom of the travertine of sampling sites H3, H4, and H5 (Fig. 1) for radioactive carbon isotope analysis.

Measurements instruments and methods

The temperature and pH were measured on-site using a multi-parameter instrument (HANNA HI 98194). Major anions, except HCO_3^- , were analyzed using ion chromatography (Dionex ICS 2500). CO_2 and HCO_3^- concentrations were measured by titration. Major cations and trace elements were analyzed using an inductively coupled plasma optical emission spectrometer (PerkinElmer Optima 8000). SiO_2 was analyzed by spectrophotometry (Shimadzu UV2500). $\delta^{18}\text{O}_{\text{H}_2\text{O}}$ and δD in the water samples were measured using a Picarro L2130-i analyzer. $\delta^{18}\text{O}_{\text{SO}_4}$ and $\delta^{34}\text{S}_{\text{SO}_4}$ were measured in a thermal conversion elemental analyzer coupled with a Finnigan MAT253 mass spectrometer. ^3H and $\delta^{14}\text{C}$ isotopes were measured with a Quantulus-1220 liquid scintillation beta spectrometer, and $\delta^{13}\text{C}$ isotopes were measured using a Finnigan MAT253 mass spectrometer. Strontium isotope compositions were measured using a MAT262 thermo-ionization mass spectrometer.

The shallow and deep water circulation characteristics of different groundwater were identified by the composition of hydrochemical ions, trace elements, and isotopic characteristics, and the groundwater origin characteristics were identified by the Gibbs graphic method. Deuterium oxygen isotopes were used to calculate the recharge elevation and source of the hot springs. A geothermometer was used to calculate the circulation depth and heat storage temperature of the hot springs. Strontium isotopes were used to identify different groundwater sources and circulation paths, sulfur isotopes were used to identify the water storage environment, and the groundwater mixing ratio was calculated by the silicon-enthalpy and Cl methods. The groundwater ages were calculated by tritium and carbon isotope analysis. A conceptual model of hydrothermal spring groundwater circulation was then established (Fig. 2).

Results and discussion

Hydrochemical features

The measured chemical constituents of the water samples are listed in Table 1. The total dissolved solids (TDS) are 711.1–

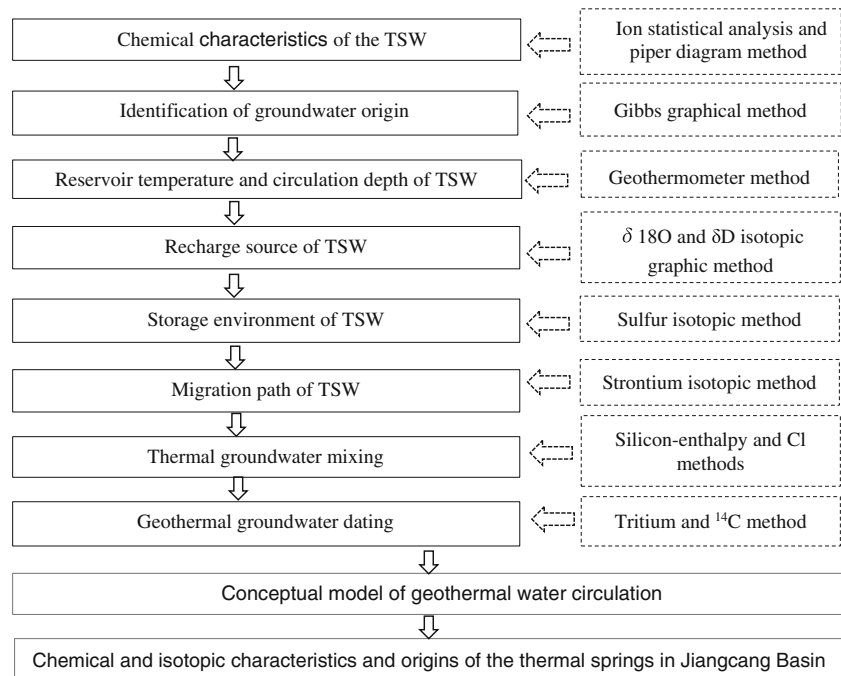
1663, 144.9–447.1, 257.5–68.8, and 312.2–646.6 mg/L for the TSW, SSW, IW, and RW, respectively. The TDS values of the TSW are substantially higher than those of the other waters, which reflects the higher contents of primary ions (except NO_3^-) and trace elements (Li, Sr, F, Ba, B, Si) and sufficient water-rock interaction (WRI) characteristics (Table 1).

The samples plot above the 1:1 in the Na^+ versus Cl^- graph shown in Fig. 3a and are distributed along two lines, which represent deep and shallow circulation where a scattered distribution is indicative of interchange. High ion concentrations represent deep WRI, whereas low ion concentrations indicate weak WRI within shallow circulation. A high Na^+/Cl^- ratio can also be attributed to WRI, such as $\text{Ca}(\text{Mg})/\text{Na}$ ionic exchange (Edmunds et al. 2003; Fu et al. 2018). Data points in the $(\text{Ca}^{2+} + \text{Mg}^{2+})$ versus $(\text{HCO}_3^- + \text{SO}_4^{2-})$ milligram equivalent diagram (Fig. 3b) generally scatter between the 1:1 and 1:2 curves, which implies that the HCO_3^- , Ca^{2+} , and Mg^{2+} ions originate mainly from the dissolution of carbonatite and gypsum (Fu et al. 2018).

Trace elements are typically used to identify groundwater with a hydrothermal origin. High trace element concentrations (e.g., Li and B in the form of HBO_2) in groundwater are indicative of geothermal springs (Li et al. 2014). As shown in Table 1, the concentrations of Li and HBO_2 for the thermal spring waters range from 0.136 to 0.975 mg/L and 8.03 to 71.85 mg/L, respectively, which are considerably higher than those measured from the other water samples. The TDS values show the same trend, which demonstrates hydrothermal origin characteristics (Fig. 3c, d). These trace elements are mainly derived from the dissolution and filtration of the fluid and surrounding rock. Higher temperatures are associated with longer flow paths, more complete WRI, and higher quantities of trace elements extracted from the surrounding rock (Li et al. 2014).

The outlet temperature (T_{spring}) and TDS values indicate that the TSW samples from the study area can be divided into three groups (Fig. 1): (1) thermal springs from the northern bank of the Datong River (TSW-N, $T_{\text{spring}} > 35$ °C, TDS < 1 g/L); (2) thermal springs in the Datong River washland (TSW-D, $T_{\text{spring}} < 20$ °C, TDS > 1.5 g/L); and (3) thermal springs from the southern bank of the Datong River (TSW-S, $T_{\text{spring}} > 20$ °C, 1.0 g/L < TDS < 1.5 g/L).

Table 1 shows the major ion concentrations in the TSW, SSW, IW, and RW. The spring vent temperatures of the TSW-N, TSW-D, and TSW-S are 35.2–36.6 °C, 8.9 °C, and 20.5–24 °C, respectively. The TDS values of the TSW-N, TSW-D, and TSW-S are 711.1–778.5, 1663, and 1233–1322 mg/L, respectively (Table 1). The salinity of the TSW-S is higher than that of the TSW-N, but the temperature is lower. The waters are distinguished on the basis of Schukalev's classification and Kurilov's formula. In

Fig. 2 Flowchart of the research methodology

particular, the TSW-N is a $\text{HCO}_3\text{-Na}\cdot\text{Ca}(\text{Ca}\cdot\text{Na})$ type, the TSW-D is a $\text{HCO}_3\text{-Ca}\cdot\text{Mg}$ type, and the TSW-S is a $\text{HCO}_3\cdot\text{SO}_4\text{-Na}\cdot\text{Ca}$ type.

The main hydrochemical types of the SSW, IW, and RW are $\text{HCO}_3\text{-Ca}(\text{Ca}\cdot\text{Mg})$, $\text{HCO}_3\cdot\text{SO}_4$, and $(\text{SO}_4\cdot\text{HCO}_3)\text{-Ca}\cdot\text{Na}$ ($\text{Na}\cdot\text{Ca}$), respectively, and clearly demonstrate mixing processes that are further verified by the linear distribution of data in the Piper diagram (Fig. 4). The data points that plot above the line indicate evaporation (SSW and RW), whereas those below the line represent deep circulation and WRI (TSW), which is accompanied by a significant increase of HCO_3^- . The TSW-S and TSW-D data points are near the hybrid lines, which indicate that they may be mixed by shallow groundwater.

Reservoir temperature and circulation depth

Silica geothermometers, cation geothermometers, and multi-mineral balance geothermometers are commonly used to estimate geothermal reservoir temperatures (Brook et al. 1979; Truesdell and Hulston 2017; Tong and Zhang 1989; Bo et al. 2015), all of which are applied on the assumption of equilibrated water. Because each geothermometer has its own limitations, it is critical to compare the results obtained from the different estimation methods. As shown in Fig. 5, the data points of the TSW, SSW, and IW all suggest immature waters (close to the $\text{Mg}^{1/2}$ end-member). Thus, the methods and protocol suggested by Brook et al. (1979), Fournier (1981), Tong and Zhang (1989), and Bo et al. (2015) were used to identify

the most credible calculated reservoir temperature (T_r) among the temperature estimates, as follows.

If $\theta\text{SiO}_2 > \theta\text{NaK} > \theta\text{NaKCa} > \theta\text{KMg}$, then $T_r = \theta\text{NaK}$
 If $\theta\text{SiO}_2 > \theta\text{NaK} > \theta\text{KMg} > \theta\text{NaKCa}$, then $T_r = \theta\text{NaK}$
 If $\theta\text{NaKCa} > \theta\text{NaK}$, then $T_r = \theta\text{SiO}_2$
 If $\theta\text{NaK} > \theta\text{SiO}_2 > \theta\text{NaKCa}$, then $T_r = \theta\text{SiO}_2$
 If $\theta\text{NaK} > \theta\text{NaKCa} > \theta\text{SiO}_2 > \theta\text{KMg}$, then $T_r = \theta\text{SiO}_2$
 If $\theta\text{NaK} > \theta\text{NaKCa} > \theta\text{KMg} > \theta\text{SiO}_2$ and $T_{\text{spring}} < 40^\circ\text{C}$, then $T_r = \theta\text{NaKCa}$

where θ_x is the reservoir temperature calculated by method x (SiO_2 , NaK , NaKCa , KMg).

Following the above rules, the calculated T_r values of the TSW-N, TSW-D, TSW-S, IW, and SSW are 62.7–72.4 °C, 91.8 °C, 81.6–91.4 °C, 23.9–37.6 °C, and 19.4–24.7 °C, respectively (Table 1). If the influence of cold groundwater is deducted, the true T_r values should be considerably higher (Table 3). The geothermal gradient of the geothermal anomaly area in the Jiangcang Basin is 4.2 °C/hm (Regional Hydrogeological Survey Report 1978, 1987) and 2 °C/hm for the SSW and IW. The circulation depths of the TSW-N, TSW-D, TSW-S, IW, and SSW are 1942–2175, 2186, 1494–1724, 569–897, and 462–577 m, respectively.

Thermal groundwater recharge source, storage environment, and migration path

The linear relationship between the $\delta^{18}\text{O}$ and δD values of the meteoric water can be used to identify the water source of a thermal spring (Zhou et al. 2008). The correlation between $\delta^{18}\text{O}$ and δD in waters (TSW, IW, SSW, and RW) of the

Table 1 Hydrochemical composition of the groundwater and river water in the Jiangcang Basin (mg/L)

Sample	TDS	K ⁺	Na ⁺	Ca ²⁺	Mg ²⁺	Cl ⁻	SO ₄ ²⁻	HCO ₃ ⁻	NO ₃ ⁻	F ⁻	SiO ₂	CO ₂	Li	Sr	Ba	HBO ₂	PH	Hydrochemical type	
Suprapermafrost spring	S1	144.9	0.8	4.94	39.65	5.15	3.5	7.11	146.44	4.11	0.24	6.75	6.12	ND	0.347	-	0.29	7.47	HCO ₃ -Ca
SSW	S2	205.1	1.42	5.87	52.66	10.02	4.76	30.0	183.05	3.3	0.27	5.73	6.12	-	-	0.24	7.57	HCO ₃ -Ca	
	S3	303.2	1.32	37.36	48.82	15.25	5.91	67.66	217.2	2.08	0.26	17.36	8.8	0.009	0.526	0.194	nd	7.53	HCO ₃ •SO ₄ -Ca•Na
	S4	396.9	0.69	91.52	30.38	6.3	3.42	212.0	89.55	2.48	0.1	5.75	3.58	0.006	0.375	0.074	nd	7.45	SO ₄ •HCO ₃ -Na•Ca
	S5	413.1	0.64	24.75	67.91	33.46	2.08	159.1	239.3	nd	0.3	5.71	6.6	0.007	0.48	0.035	0.28	7.7	HCO ₃ •SO ₄ -Ca•Mg
	S6	447.1	1.18	100.5	35.05	9.55	8.54	212.5	144.5	1.2	0.14	6.85	7.15	nd	0.217	0.040	nd	7.35	SO ₄ •HCO ₃ -Na•Ca
	X1	468.8	2.77	49.66	88.92	24.06	11.94	79.57	397.8	1.4	nd	8.57	13.2	0.032	0.614	0.112	5.29	7.62	HCO ₃ -Ca•Na
Infrafermafrost water	X2	257.5	1.13	38.84	42.72	9.2	4.73	71.95	164.5	3.16	0.1	7.65	6.6	0.008	0.236	0.051	0.64	7.53	HCO ₃ •SO ₄ -Ca•Na
	X3	351.7	1.46	73.48	37.17	8.07	5.25	145.9	141.1	3.08	0.26	6.68	4.44	0.010	0.258	0.033	0.34	7.64	SO ₄ •HCO ₃ -Na•Ca
	X4	288.0	1.66	30.01	50.82	14.92	7.18	62.95	213.6	2.8	0.22	10.46	4.44	0.020	0.212	0.065	1.06	7.81	HCO ₃ •SO ₄ -Ca•Na
	X5	437.5	1.52	72.78	61.44	12.63	8.75	152.4	216.2	11	0.12	9.31	2.22	0.008	0.294	0.198	0.29	8.13	HCO ₃ •SO ₄ -Na•Ca
	H1	711.1	11.82	133.8	62.08	35.62	70.05	108.6	465.7	1.36	2.2	34.72	8.8	0.136	0.554	0.248	29.12	7.86	HCO ₃ -Na•Ca
Thermal Spring Water TSW	H2	778.5	11.96	157	55.18	34.96	66.97	175.3	406	0.78	2.4	35.68	ND	0.134	0.544	0.331	28.92	8.64	HCO ₃ -Na•Ca
	H3	720.4	12.78	91.08	105.1	38.87	71.78	29.7	612.9	0.26	2.0	43.61	26.01	0.146	0.692	0.512	30.97	7.51	HCO ₃ -Ca•Na
	H4	1663	74.55	172.5	267.6	92.5	165.3	56.74	1474	0.72	1.1	44.05	143.1	0.975	2.854	0.295	71.85	7.08	HCO ₃ -Ca•Mg
	H5	1233	18.79	163.2	141.3	73.89	59.8	321.1	770.1	nd	1.4	27.73	32.19	0.466	1.143	0.039	58.8	7.43	HCO ₃ •SO ₄ -Na•Ca
River water	H6	1268	17.66	199	173.2	47.15	52.96	329.7	776.1	0.92	1.0	14.32	21.46	0.47	1.235	0.032	63.95	7.61	HCO ₃ •SO ₄ -Na•Ca
	H7	1322	33.41	202.1	166.8	68.4	79.48	320.3	836.5	0.56	2.4	22.72	46.67	0.708	2.196	0.056	8.03	7.39	HCO ₃ •SO ₄ -Na•Ca
	R1	374.6	1.69	45.74	60.69	14.92	12.95	125.8	206.3	3.88	0.18	6.07	4.33	0.007	0.293	0.057	ND	7.81	HCO ₃ •SO ₄ -Ca•Na
RW	R2	312.1	1.57	37.54	54.08	14.04	12.87	82.43	197.4	2.84	0.18	8.65	4.4	0.01	0.39	0.089	ND	7.79	HCO ₃ •SO ₄ -Ca•Na
	R3	646.6	0.87	147.4	48.22	10.5	5.25	342.5	170.9	2.44	0.10	4.22	6.5	0.01	0.308	0.066	ND	7.56	SO ₄ •HCO ₃ -Na•Ca

“ND” indicates that the concentration was below the detection limit; “-” indicates that the concentration was not detected

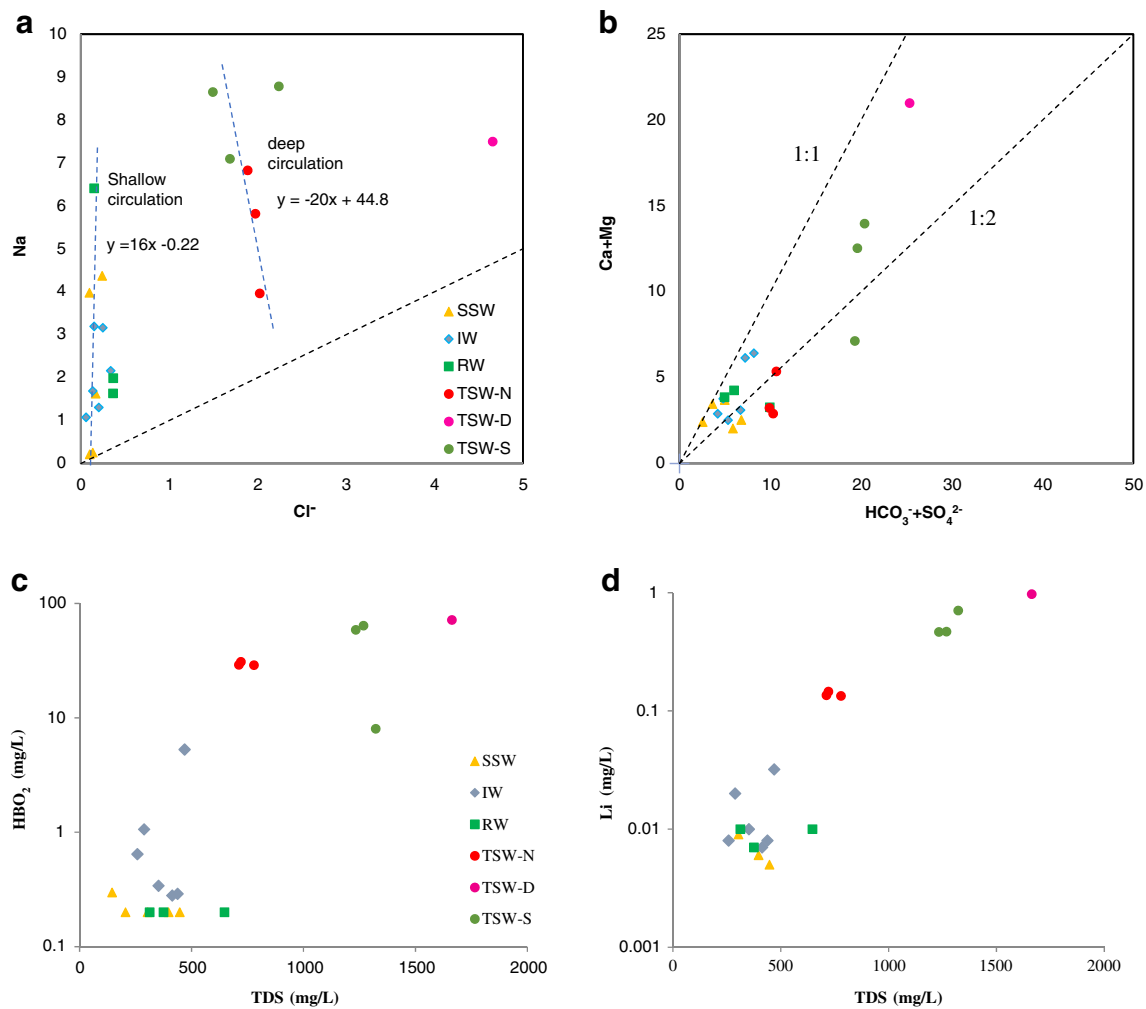


Fig. 3 **a** Na^+ versus Cl^- . **b** $(\text{Ca}^{2+} + \text{Mg}^{2+})$ versus $(\text{HCO}_3^- + \text{SO}_4^{2-})$, expressed in $\text{mol}\cdot\text{L}^{-1}$. **c** HBO_2 versus total dissolved solids (TDS), expressed in $\text{mg}\cdot\text{L}^{-1}$. **d** Li versus TDS, expressed in $\text{mg}\cdot\text{L}^{-1}$

Jiangcang Basin is shown in Fig. 6a alongside the local Yeniugou meteoric water line (LMWL: $\delta\text{D} = 7.65 \times \delta^{18}\text{O} + 12.4$) (Zhao et al. 2011) and global meteoric water line (GMWL: $\delta\text{D} = 8 \times \delta^{18}\text{O} + 10$) (Craig 1961). The data are consistent with the regional meteoric line, which indicates that the waters in the study area are recharged by meteoric precipitation. The $\delta^{18}\text{O}$ and δD values of the TSW are -10 to -8‰ and -65 to -55‰ , respectively, which are considerably lower than the other waters (IW, SSW, RW), implying deep groundwater circulation.

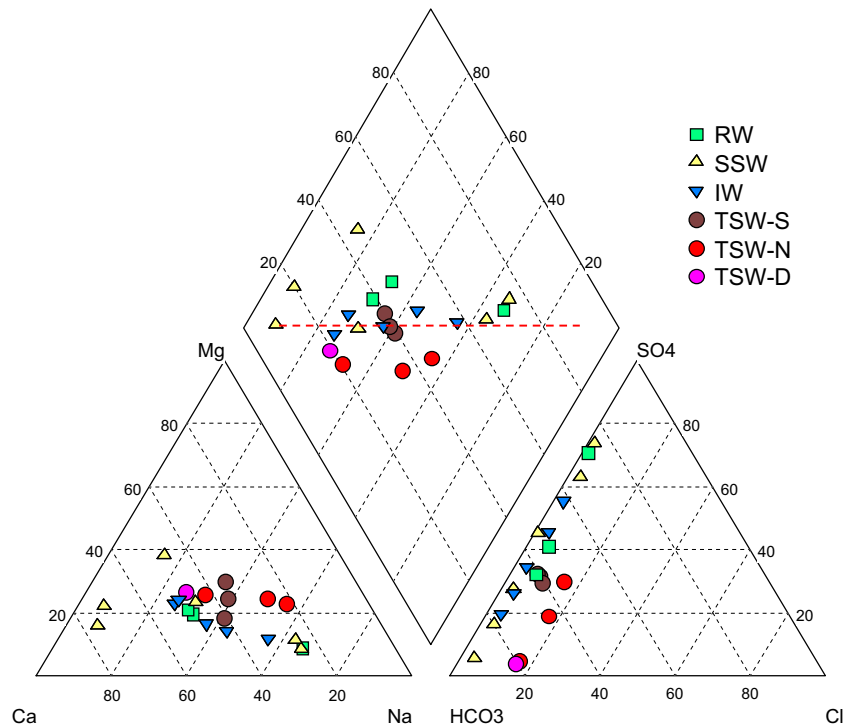
Isotopic exchange between the deep circulating water and surrounding rock leads to a shift of $\delta^{18}\text{O}$ (Bo et al. 2015), the degree to which depends on the circulation depth, reservoir temperature, and WRI efficiency (Vonsée et al. 2019; Davraz 2008). Only the thermal springs show a slight oxygen shift (Fig. 6a). The degree of the $\delta^{18}\text{O}$ shift for the TSW-S, TSW-N, and TSW-D increases linearly ($\delta\text{D} = 2.2474 \times \delta^{18}\text{O} - 40.674$, $n = 7$), which indicates that they are controlled by circulation depth (TSW-S < TSW-N < TSW-D).

Altitude effects on the hydrogen-oxygen isotopic data are observed in the Jiangcang Basin. The relationship between δD values and groundwater altitude (IW, SSW) can be expressed by the regression line, Elevation (m) = $-13.774\delta\text{D} + 3227$ ($n = 13$, $R^2 = 0.639$) (Fig. 6b). The thermal spring samples plot on the lower left side of the trend line, implying that these recharge areas differ from those of the IW and SSW.

In the $\delta^{18}\text{O}$ versus Cl^- diagram (Fig. 6c), the distribution characteristics of the thermal spring samples differ from those of the cold water samples. These findings indicate that the variations in Cl^- concentrations and isotope composition of the thermal springs and cold water can mainly be attributed to different sources and water recharge elevations (Tan et al. 2014).

The recharge elevation of the major thermal springs can be calculated by the isotope elevation effect from precipitation in the study area. Precipitation samples were not collected at different elevations in this study; thus, previous statistical results (Elevation = $927 - 56.8\delta\text{D}$) were adopted for the

Fig. 4 Piper diagram of hydrochemical types from different waters

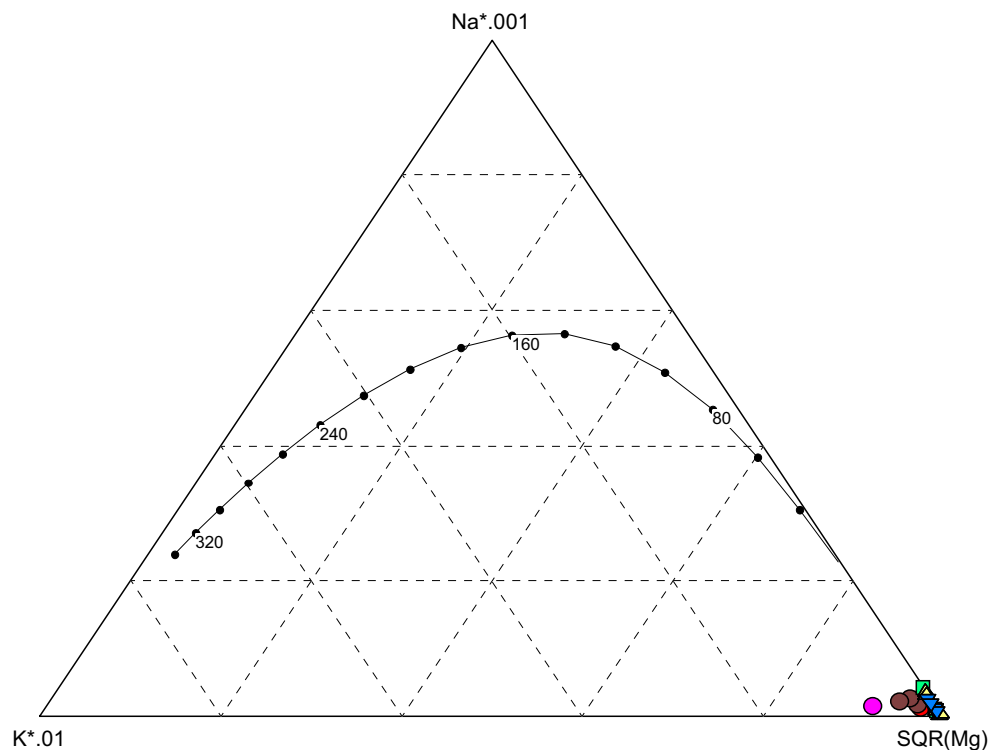


calculations (Liu 2013). The results listed in Table 2 show that the recharge altitudes of the TSW-N, TSW-D, and TSW-S are 4335–4505, 4335, and 4278–4505 m, respectively, which are approximately 600 m higher than the elevation of the springs points. This difference indicates that the thermal springs are

recharged in high-altitude mountains, namely, the Datong Mountains and Tuolai Mountains.

The $\delta^{34}\text{S}$ values of SO_4^{2-} from the TSW, SSW, IW, and RW range from 12.4 to 14.4‰, 9.6‰, 13.7 to 13.8‰, and 10.4 to 12.6‰, respectively. The $\delta^{18}\text{O}$ values of SO_4^{2-} from

Fig. 5 Na-K-Mg trilinear equilibrium diagram for hydrothermal water



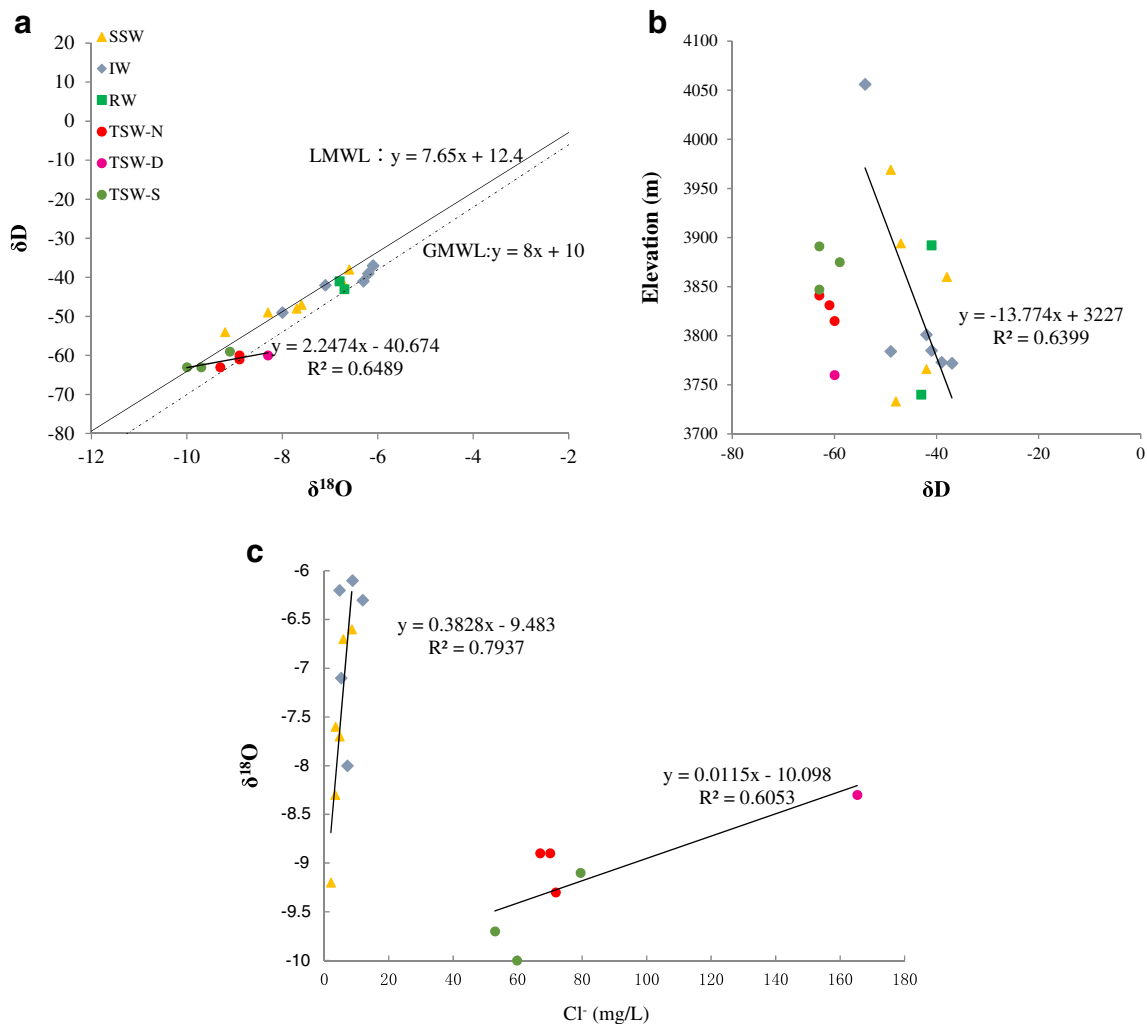


Fig. 6 a δD versus $\delta^{18}O$. b δD versus elevation. c $\delta^{18}O$ versus Cl^-

the TSW, SSW, IW, and RW range from 14.0 to 17.4‰, 15.5‰, 13.0 to 15.7‰, and 15.2 to 15.7‰, respectively. On a $\delta^{18}O-SO_4^{2-}$ versus $\delta^{18}O-H_2O$ diagram, the SO_4^{2-} derived from sulfide oxidation must fall into the experimental area defined by Van Stempvoort and Krouse (1994). Figure 7a shows that all of the water samples from the Jiangcang Basin plot outside of the experimental area, indicating limited organic sulfur and sulfide oxidation contributions to the groundwater sulfate in the study area.

The groundwater can be divided into three groups, as shown in Fig. 7b. Group I has low SO_4^{2-} contents and high $\delta^{34}S$, indicating that the reduced groundwater SO_4^{2-} is mainly caused by reduction in a closed environment. Group II has high SO_4^{2-} contents and $\delta^{34}S$, indicating that the groundwater leached from SO_4^{2-} -rich rocks, as represented by the Zemoyesang spring (H5). The hydrogeological conditions of the geothermal zone are therefore closer to those in an open system, which provides a continuous supply of SO_4^{2-} . Group III has high SO_4^{2-} contents and low $\delta^{34}S$, indicating that the groundwater is in an open oxidation environment (Li et al. 2014).

Figure 6c and d show a linear increase of $\delta^{34}S$ with decreasing SO_4^{2-}/Cl^- over the full range of study, whereas $\delta^{18}O$ values remain essentially constant at 18–20‰ below a SO_4^{2-}/Cl^- ratio of ~ 0.1 . This implies that bacterial sulfate reduction (BSR) is responsible for the groundwater isotopic composition (Zsolt et al. 2002; Li et al. 2014). The group I springs (TSW-N and TSW-D) are representative of the BSR process and contain less SO_4^{2-} than the other waters.

Strontium isotopes are useful tracers to identify the migration path of groundwater (Khadija et al. 2017; Han and Liu 2004; Wang et al. 2007). Unlike many stable isotopes, the $^{87}Sr/^{86}Sr$ ratio does not change with altitude, latitude, or evaporation and reflects interactions between the groundwater and surrounding rocks (Khadija et al. 2017). Silicate rocks commonly have higher $^{87}Sr/^{86}Sr$ (> 0.715) and lower Sr contents (Han and Liu 2004; Wang et al. 2007), whereas carbonate rocks have lower $^{87}Sr/^{86}Sr$ (~ 0.709) and higher Sr contents (Khadija et al. 2017). Figure 8 shows $^{87}Sr/^{86}Sr$ versus Sr and $1/Sr$ for the water samples collected from the Jiangcang Basin.

Table 2 Isotopic composition of the groundwater and river water in the Jianggang Basin

Sample	EI* m	T _{spring} °C	T _{Reservoir} ^Δ °C	Circulation depth * _z (m)	D‰ vs SMOW	O‰ vs SMOW	Recharge EI* (m)	d- excess	T	¹³ C (‰)	¹⁴ C(pmc)	¹⁴ C (ka)	Tamers (a)	Fontes and Garnier (a)	δ ³⁴ S _{SO4} (‰, VCDT)	δ ¹⁸ O _{v.} SMOW (‰)	⁸⁷ Sr/ ⁸⁶ Sr
S1	3894	4	24.3	577	-47	-7.6	-	13.8	-	-13.5	-	0.1588	-	-	-	-	0.7118
S2	3733	5	19.5	464	-48	-7.7	-	13.6	-	-	-	-	-	-	-	-	0.7121
S3	3766	3.5	23.0	547	-42	-6.7	-	11.6	-	-	-	-	-	-	-	-	-
S4	3969	4.6	19.6	467	-49	-8.3	-	17.4	27.1	-	-	-	-	-	-	-	-
S5	4056	5	19.4	462	-54	-9.2	-	19.6	26.7	-7.2	-	12.00	-	-	9.6	15.5	-
S6	3860	1.8	24.7	588	-38	-6.6	-	14.8	24.9	-	-	-	-	-	-	-	-
X1	3785	5.7	31.4	748	-41	-6.3	-	9.4	24.7	-	-	-	-	-	-	-	-
X2	3773	7.8	27.9	666	-39	-4.2	-	-5.4	37.8	-7.8	-	3.43	-	-	--	-	-
X3	3801	3.8	23.9	569	-42	-7.1	-	14.8	34.7	-6.6	60.02	4.22	-1334	8699	13.7	15.7	0.7114
X4	3784	3	37.6	897	-49	-8	-	15	26.6	-	-	10.84	-	-	-	-	0.7121
X5	3772	2	34.0	809	-37	-6.1	-	11.8	30.5	-	36.97	8.23	2537	6889	13.8	13	0.7123
H1	3815	35.2	81.6	1942	-60	-8.9	4335	11.2	3.4	-	-	-	-	-	-	-	0.7169
H2	3831	35.8	82.7	1969	-61	-8.9	4392	10.2	3.4	-	-	-	-	-	-	-	0.7173
H3	3841	36.6	91.4	2175	-63	-9.3	4505	11.4	2	-1.4	0.86	39.29	33586	39600	12.8	17.4	0.7173
H4	3760	8.9	91.8	2186	-60	-8.3	4335	6.4	4.9	3.7	13.32	16.66	11303	8305	14.2	16.1	0.7113
H5	3891	24	72.4	1724	-63	-10	4505	17	0.5	1.5	2.25	31.38	25800	27846	12.4	14	0.7135
H6	3847	21	62.7	1494	-63	-9.7	4505	14.6	2.1	-	-	-	-	-	-	-	-
H7	3875	20.5	64.7	1541	-59	-9.1	4278	13.8	4.3	--	1.29	35.9	30452	30452	14.4	16.2	-
R1	3760	-	-	-	-	-	-	-	-	-	-	-	-	-	12.6	15.7	0.7120
R2	3760	-	-	-	-43	-6.7	-	10.6	21.5	-	-	-	-	-	-	-	0.7118
R3	3892	-	-	-	-41	-6.8	-	13.4	27	-	-	-	-	-	10.4	15.2	-

“ND” indicates that the concentration was below the detection limit; “-” indicates that the concentration was not detected

*Represents elevation

^Δ Represents reservoir temperature

*_z Represents groundwater circulation depth

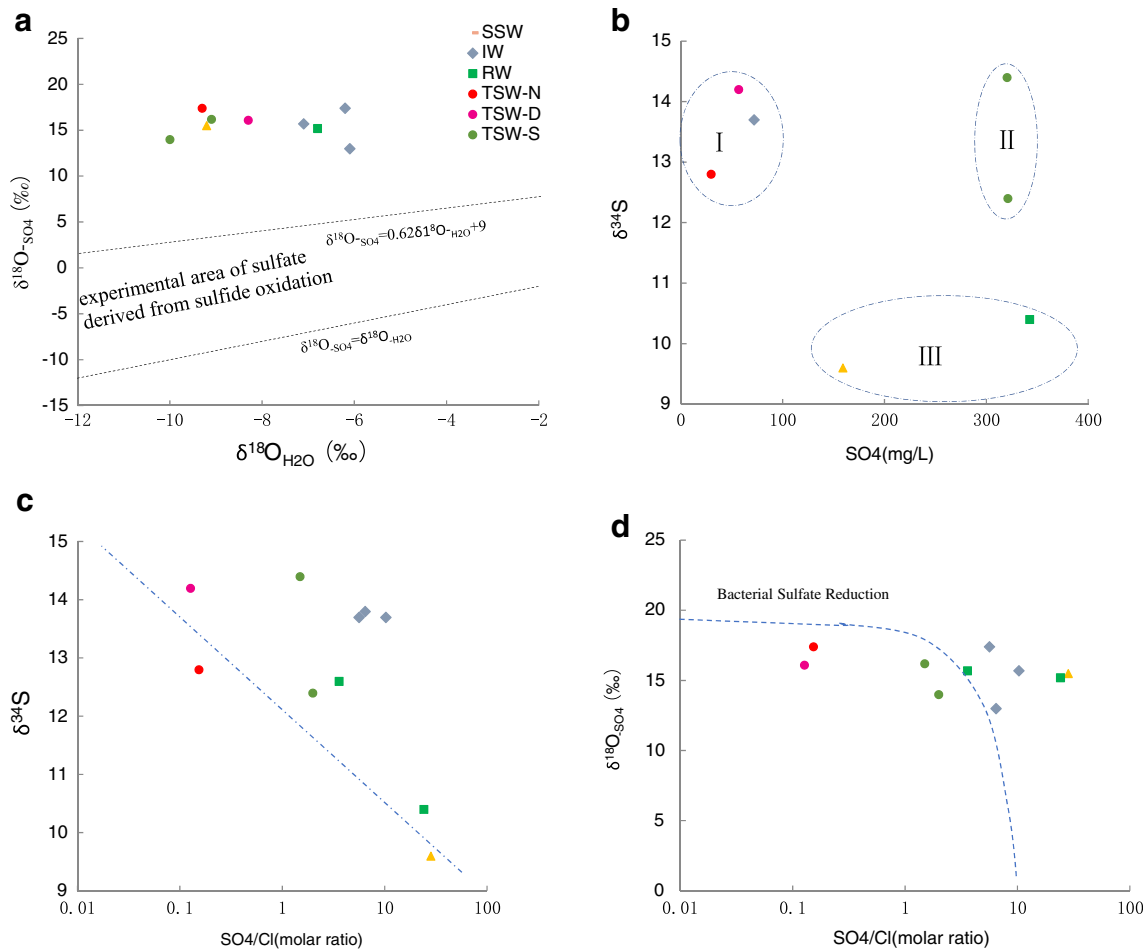


Fig. 7 a $\delta^{18}\text{O}_{\text{SO}_4}$ versus $\delta^{18}\text{O}_{\text{H}_2\text{O}}$. b $\delta^{34}\text{S}$ versus SO_4^{2-} . c $\delta^{34}\text{S}$ versus $\text{SO}_4^{2-}/\text{Cl}^-$. d $\delta^{18}\text{O}_{\text{SO}_4}$ versus $\text{SO}_4^{2-}/\text{Cl}^-$ (molar ratio)

The IW, SSW, and RW with low Sr contents (0.035–0.614 mg/L) and low $^{87}\text{Sr}/^{86}\text{Sr}$ (0.7114–0.7123) indicate that the Sr source comes from shallow circulation through evaporites or carbonates (Fig. 8a and Table 2). The thermal springs originate from varied sources with $^{87}\text{Sr}/^{86}\text{Sr}$ values ranging

from 0.7113 to 0.7173 and Sr contents between 0.544 and 2.854 mg/L, which are higher than the other waters and thus indicative of stronger WRI. The TSW-N has a high $^{87}\text{Sr}/^{86}\text{Sr}$ ratio (0.7169–0.7173), low Sr contents (0.544–0.692 mg/L), and high SiO_2 contents (Table 1), which are likely mainly

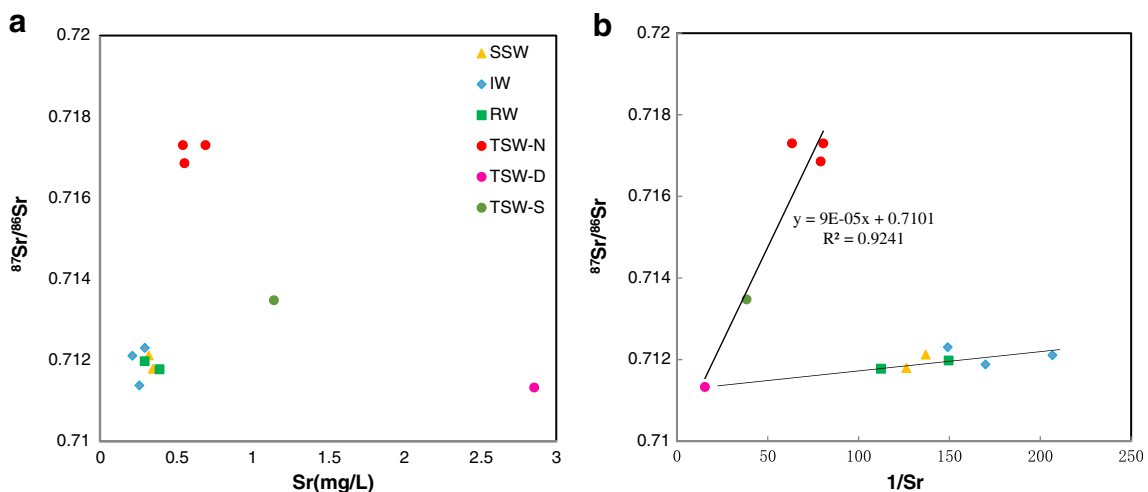


Fig. 8 a $^{87}\text{Sr}/^{86}\text{Sr}$ versus Sr and b $1/\text{Sr}$

derived from silicates. The TSW-D shows low $^{87}\text{Sr}/^{86}\text{Sr}$ (0.7113) and high Sr contents (2.854 mg/L), which indicate deep meteoric water circulation through carbonates.

The Sr data from the IW, SSW, RW, and TSW-D samples show different linear distributions (Fig. 8b). The $^{87}\text{Sr}/^{86}\text{Sr}$ ratios remain essentially unchanged (~ 0.712) with increasing Sr, indicating the interaction of the IW, SSW, RW, and TSW-D and possibly a consistent carbonate source (Odum 1957; Fan et al. 2019). Based on the local geological background, the waters can infiltrate along the NW-trending faults (F_7); thus, the river melt zone in the upper reaches of the basin is one of the supply channels for the TSW-D. In contrast, a strong positive correlation is observed between $^{87}\text{Sr}/^{86}\text{Sr}$ and $1/\text{Sr}$ in the TSW data, which show two mixing end-members: a carbonate source (TSW-D) to a silicate source (TSW-N).

Thermal groundwater mixing

The silicon-enthalpy method (Truesdell and Fournier 1977) can be used to evaluate the composition and reservoir temperature of deep thermal groundwater. As listed in Table 3, the enthalpy of the thermal spring and cold groundwater can be found in steam tables (Keenan et al. 1969). In this study, the cold spring S2 was taken as a shallow cold groundwater end-member. Assuming SiO_2 is saturated in deep groundwater, the enthalpy values and saturated SiO_2 contents can be determined by the graphic method (Fig. 9). Steam separation (boiling) occurs prior to mixing at 88 °C (local boiling point), and silica and enthalpy values can be extracted from the intersection of the quartz solubility curve and the constant enthalpy line (i.e., horizontal extension; 88 °C, 369 kJ/kg) from the intersection point of the mixing line that joins the thermal springs to the cold water (Table 3) (Zhao et al. 2018).

Because Cl^- is conservative, it can also be used to calculate the mixing ratio of thermal groundwater as a natural tracer (Li et al. 2014; Zhao et al. 2018). The deep thermal groundwater chloride concentration was calculated on the basis of the relationship between chloride concentration and temperature (Li

et al. 2014) ($C_{\text{Cl}} = 2.0853 \times T - 1.6837$, $n = 16$ in this study). The mixing ratios were calculated by the two following methods using the binary mixing model of mass conservation, which are expressed as:

$$\begin{aligned} ScX + Sh(1-X) &= Sm \\ \text{SiO}_2cX + \text{SiO}_2h(1-X) &= \text{SiO}_2m \\ \text{Cl}cX + \text{Cl}h(1-X) &= \text{Cl}m \end{aligned}$$

where Sc , Sm , and Sh are the enthalpies of the cold groundwater (S2, 21.6 kJ/kg), thermal spring water, and deep thermal groundwater, respectively; SiO_2c , SiO_2m , and SiO_2h are the SiO_2 concentrations in the cold groundwater (S2, 5.73 mg/kg), thermal spring water, and deep thermal groundwater, respectively; $\text{Cl}c$, $\text{Cl}h$, and $\text{Cl}m$ are the Cl^- concentrations in the cold groundwater (S2, 4.76 mg/L), thermal spring water, and deep thermal groundwater, respectively; and X is the mixture ratio (Zhao et al. 2018).

The results show that the cold groundwater mixture ratio for the TSW-N obtained from the two methods is similar: ~ 60.1 – 65.8% (Table 2). The cold groundwater mixture ratio of the TSW-D calculated by the silica-enthalpy method is 91.0%, whereas that obtained using the Cl method is 13.3%. The former result is considered more accurate because of the considerable amount of cold water that cools the Datonghe spring. The cold groundwater mixture ratio of the TSW-S calculated by the silica enthalpy method (76.6–79.7%) is higher than that calculated using the Cl method (51.8–61.9%), and the latter is considered more accurate because the cold water in the southern Datonghe bank is less than that in the northern bank owing to thinner seasonal melting depth in the former. The reservoir temperature calculated by the silica-enthalpy method is higher than that obtained by the Na-K-Ca geothermometer method, which reflects the maximum temperature of the deep heat storage (Tables 1 and 2).

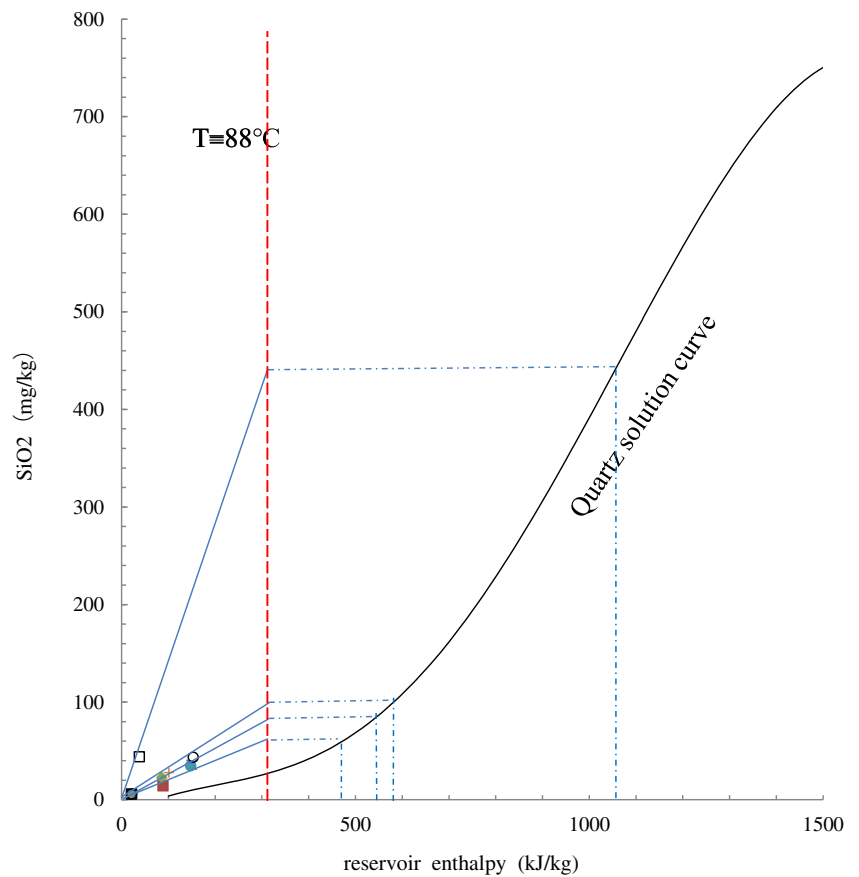
Geothermal groundwater dating

Tritium is used to assess groundwater residence times. Tritium concentrations below 1 TU imply old water (> 50 years), and

Table 3 Cold groundwater mixture ratios of the thermal springs determined by silica-enthalpy and Cl methods

ID	T_{spring} (°C)	T_r geothermometer (°C)	Reservoir enthalpy (kJ/kg)	SiO_2 in deep thermal water (mg/kg)	T_r silica-enthalpy method (°C)	Shallow water (%) silica-enthalpy method	Shallow water (%) Cl
H1	35.2	81.6	525	90.5	125	65.8	60.1
H2	35.8	82.7	536	91	127.5	64.9	62.5
H3	36.6	91.4	575	102	136	60.6	63.6
H4	8.9	91.8	1030	700	237	91.0	13.3
H5	24	72.4	570	100	135	76.6	61.9
H6	21	62.7	415	48	99	79.7	61.2
H7	20.5	64.7	520	79	123.5	76.8	51.8

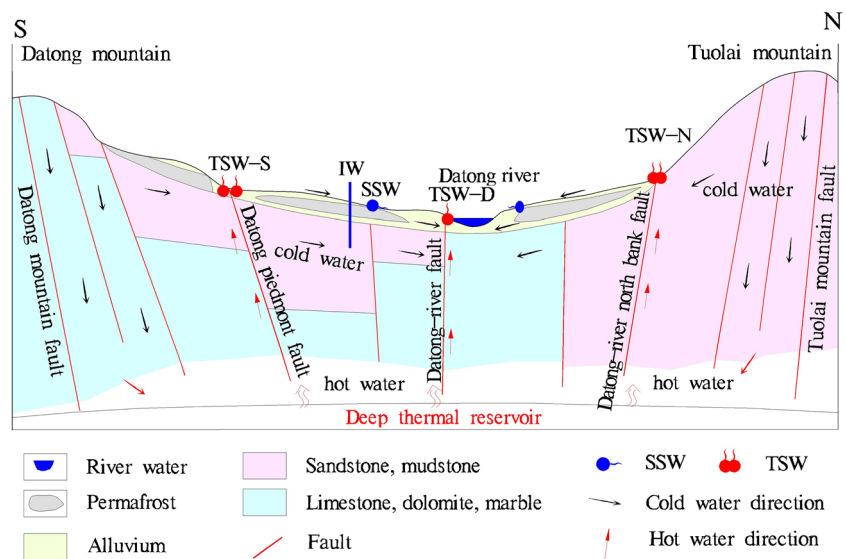
Fig. 9 SiO₂ versus enthalpy



values between 1 and 8 TU indicate a mixture of old water and new water (Ravikumar and Somashekar 2011). The tritium values for the thermal waters in the Jiangcang Basin range from 0.5 to 4.3 TU. The Zemoyesang spring (0.5 TU) therefore contains old water, and the other thermal springs are a mixture of old and more recent waters (Table 2).

¹⁴C dating is a technique used to determine the formation age of relatively old groundwater with an upper limit of ~ 50,000 years. The measured radiocarbon values of the water must be corrected to obtain reliable results. The corrected radiocarbon ages are compared using a chemical mixing model (Tamers 1975), isotope mixing model (Pearson 1965;

Fig. 10 Conceptual model of geothermal water circulation



Pearson and Hanshaw 1970), and general isotope mixing exchange model (Fontes and Garnier 1979). The results obtained from these three methods are similar. According to the corrected ^{14}C age (Table 2), the formation age of the thermal springs is between 8699 and 39,600 years. The oldest age is between 33,586 and 39,600 years in the Muliqugu spring (H3), and the youngest age is between 8305 and 11,303 years in the Datonghe spring (H4), which is likely related to the mixing of modern waters.

Conceptual model of geothermal water circulation

A conceptual model of the occurrence of thermal springs in the region is proposed based on the hydrogeochemical results and hydrogeological features. Meteoric precipitation and melting water from ice and snow infiltrate through the fold fracture zones above 4,300 m in areas along Tuolai Mountain and Datong Mountain and groundwater runoff along the structural channel. Below ~2000-m deep circulation, the groundwater is heated by a deep heat source and exposed in the form of thermal springs along some fault complex zones. Most thermal springs pass through permafrost and melt areas of rivers and are mixed and cooled by the shallow cold groundwater, especially the Datonghe spring (Fig. 10).

Conclusions

The thermal springs in the Jiangcang Basin occur in the northern Qilian orogenic belt geothermal zone, which is a typical geothermal zone on the northeastern edge of the Qinghai-Tibet Plateau. (1) The chemical and isotopic results indicate that the thermal springs in this region are of meteoric origin. The circulation depth, flowing pathway, residence time, and mixing relationship with cold water lead to different characteristics between the TWS-S, TWS-N, and TSW-D. (2) The TSW-S is exposed in bands with TDS up to 1 g/L along the Datong Mountain piedmont fault, recharged from Datong Mountain (4278–4505 m), flows through carbonates, and mixes with the shallow circulating cold water (51.8–61.9%) in the southern bank. The TSW-D is exposed along the Datong River fault with high TDS (> 1.5 g/L) and low temperature (< 20 °C), recharged from Datong Mountain (4335–4505 m) and the upper reaches of the river melt zone, flows through carbonates, and mixes with SSW and RW (91.0%) in the Datong River floodplain. The TSW-N is exposed at the Datong River northern bank fault with temperatures above 35 °C and TDS < 1 g/L, recharged from Tuolai Mountain (4335–4505 m) thermal water flowing through silicates, and mixes with the shallow circulating cold water (60.1–65.8%) in the northern bank. (3) Two new findings that were not evident in previous studies were obtained, which

confirm the recharge migration route of these three different type thermal springs. The TSW-D and TSW-S are mainly derived from carbonate rocks, and the TSW-N is from silicates. The TSW-N and TSW-D are in a closed reducing environment with deeper circulation depths (1942–2186 m), whereas the TSW-S is in a relatively open system with a shallow circulation depth (1494–1724 m).

It is recommended that a reservoir be built at the mouth of the TSW-N and wells can be drilled next to the TSW-D and TSW-S through cold water aquifers to obtain deep hot water for geothermal energy. These results and suggestions provide important information for the use and management of geothermal resources in the Datong River Basin.

Acknowledgments We thank Esther Posner, PhD, from Liwen Bianji, Edanz Editing China (www.liwenbianji.cn/ac), for editing the English text of a draft of this manuscript.

Code availability Not applicable.

Authors' contributions Wang Zhenxing initialized the study, interpreted the data, and wrote the manuscript. Li Xiangquan helped design the experiments and analyze the data.

Funding This research was funded by the National Natural Science Foundation of China (NSFC, Grant No. 41302190).

Data availability Not applicable.

Declarations

Conflict of interest The authors declare that they have no conflict of interest.

References

- Bo Y, Liu CL, Zhao YJ, Wang LC (2015) Chemical and isotopic characteristics and origin of spring waters in the Lanping–Simao Basin, Yunnan, Southwestern China. *Chemie der Erde* 75:287–300
- Brook CA, Marina RH, Mabey DR (1979) Hydrothermal convection systems with reservoir temperature ≥ 90 °C. Assessment of geothermal resources of the United States – 1978. *Geol. Surv. Circ* 790:18–85
- Caron ME, Grasby SE, Cathryn RM (2008) Spring water trace element geochemistry: a tool for resource assessment and reconnaissance mineral exploration. *Appl. Geochem* 23:3561–3578
- Chatterjee S, Sinhal UK, Deodhar AS, Md Arzoo A, Nathu S, Ajay KS, Aggarwal RK, Ashutosh D (2017) Isotope–geochemical characterization and geothermometrical modeling of Uttarakhand geothermal field, India. *Environ. Earth Sci* 76:638
- Chen XH, Shao ZG, Xiong XS, Gao R, Liu XJ, Wang CF, Li B, Wang ZZ, Zhang YP (2019) Fault system, deep structure and tectonic evolution of the Qilian Orogenic Belt, Northwest China. *Geology in China* 46(5):995–1020 (in Chinese with English abstract)
- Craig H (1961) Isotopic variations in meteoric waters. *Science* 133(3465):1702–1703
- Davraz A (2008) Hydrogeochemical and hydrogeological investigations of thermal waters in the Usak Area (Turkey). *Environ. Geol* 04. 54(3):615–628

- Edmunds WM, Guendouz AH, Mamou A, Moulla A, Shand P, Zouari K (2003) Groundwater evolution in the Continental Intercalaire aquifer of southern Algeria and Tunisia: trace element and isotopic indicators. *Appl. Geochem* 18(6):805–822
- Fan YF, Pang ZH, Liao DW, Tian J, Hao YL, Huang TM, Li YM (2019) Hydrogeochemical characteristics and Genesis of geothermal water from the Ganzhi geothermal field, eastern Tibetan Plateau. *Water* 11: 1631. <https://doi.org/10.3390/w11081631>
- Favara RO, Grassa F, Inguaggiato S, Valenza M (2001) Hydrogeochemistry and stable isotopes of thermal springs: earthquake-related chemical changes along Belice Fault (Western Sicily). *Appl. Geochem.* 16:1–17
- Fontes JC, Garnier JM (1979) Determination of the initial ^{14}C activity of the total dissolved carbon: a review of the existing models and a new approach. *Water. Resour. Res* 15:399–413
- Fournier RO (1981) Application of water geochemistry to geothermal exploration and reservoir engineering. In: Rybach L, Muffler LJP (eds) *Geothermal Systems: Principles and Case Histories*. John Wiley and Sons Ltd., New York, pp 109–143
- Fu CC, Li XQ, Ma JF, Liu LX, Gao M, Bai ZX (2018) A hydrochemistry and multi-isotopic study of groundwater origin and hydrochemical evolution in the middle reaches of the Kuye River basin. *Appl. Geochem.* 98:82–93
- Gibson ML, Hinman NW (2013) Mixing of hydrothermal water and groundwater near hot springs, Yellowstone National Park (USA): hydrology and geochemistry. *Hydrol. J.* 21:919–933
- Giggenbach WF (1988) Geothermal solute equilibria. Derivation of Na–K–Mg–Ca geothermometers. *Geochim. Cosmochim. Acta* 52:2749–2765
- Giggenbach WF, Gonfiantini R, Jangi BL, Truesdell AH (1983) Isotopic and chemical composition of parbati valley geothermal discharges, North-West Himalaya, India. *Geotherm* 12:199–222
- Han G, Liu CQ (2004) Water geochemistry controlled by carbonate dissolution: a study of the river waters draining karst-dominated terrain, Guizhou province, China. *Chem. Geol.* 204(1):1–21. <https://doi.org/10.1016/j.chemgeo.2003.09.009>
- Jonathan GW, Jonathan BS, Bogdan PO (2010) Sulfur isotopic composition and the source of dissolved sulfur species in thermo-mineral springs of the Cerna Valley, Romania. *Chem Geol* 271:31–43
- Keenan JH, Keyes FG, Hill PG, Moore JG (1969) *Steam tables (International Edition-Metric Units)*. John Wiley, New York, p 162
- Khadija S, Osman A, Rashid AA, Talal AH, Clark ID (2017) Strontium isotopes as a tool for estimation of groundwater recharge and aquifer connectivity. *Groundw Sustain Dev* 4:1–11
- Li HD, Zhang SQ, Bai JQ, Zhou JY, Shi WD, Zhao Y (2007) Hydrochemistry and origin of the Yaoshuitan geothermal field, Xining, Qinghai. *Acta Geologica Sinica* 81:1299–1304
- Li XQ, Hou XW, Zhou ZC, Liu LX (2014) Geochemical characterization and origins of the thermal springs in southern Gaoligong Mountains, China. *Environ. Earth Sci* 72:3089–3098
- Liu YG (2013) Using hydrochemical and isotope tracers analyzing to delineate hydrologic process in cold alpine watershed in rainy season. PhD thesis in CNKI 4:27–30
- Liu YP, Zhou X, Deng ZJ, Fang B, Tsutomu Y, Zhao JB, Wang XC (2015) Hydrochemical characteristics and genesis analysis of the Jifei hot spring in Yunnan, southwestern China. *Geothermics* 53: 38–45
- Odom HT (1957) Strontium in natural waters. *Inst. Mar. Sci.* 4:22–37
- Pearson FJ (1965) Use of C-13/C-12 ratios to correct radiocarbon ages of material initially diluted by Limestone. In: *Radiocarbon and Tritium Dating, Proceedings of the Sixth International Conference on Radiocarbon*. Pullman Washington, pp. 357–366.
- Pearson FJ, Hanshaw BB (1970) Sources of dissolved carbonate species in groundwater and their effects on carbon-14 dating. In: *Isotopehydrology*. IAEA, Vienna, pp 271–286
- Qi JH, Li X, Xu M, Yi L, Zhang Q, Qin LM, Li KD (2018) Origin of saline springs in Yanjing, Tibet: Hydrochemical and isotopic characteristics. *Appl. Geochem* 98:164–176
- Ravikumar P, Somashekar RK (2011) Environmental tritium (^3H) and hydrochemical investigations to evaluate groundwater in Varahi and Markandeya river basins, Karnataka, India. *J. Environ. Radioact* 102(2):153–162
- Regional hydrogeological survey report of Yeniutai, 1978, 1:200000, (In Chinese).
- Regional hydrogeological survey report of Zhihema, 1987, 1:200000, (In Chinese).
- Sabria K, Marrero-Diaz R, Ntarmouchanta A, Bento dos Santos T, Ribeiro ML, Solá AR, Smaili H, Benslimanea A, Chibout M, Pérez NM, Padrón E, Melián GV, Asensio-Ramos M, Carreira PM, Jesus AP (2019) Geology and hydrogeochemistry of the thermo-mineral waters of the South Rif Thrust (Northern Morocco). *Geothermics* 78:28–49
- Song S, Niu Y, Su L, Xia X (2013) Tectonics of the North Qilian orogen, NW China. *Gondwana Res* 23:1378–1401
- Tamers MA (1975) Validity of radiocarbon dates on ground water. *Surv. Geophys* 2(2):217–239
- Tan HB, Zhang W, Chen J, Jiang S, Kong N (2012) Isotope and geochemical studies for a geothermal assessment of the Xining basin and adjacent areas, northeastern Tibetan Plateau. *Geothermics* 42: 47–55
- Tan H, Zhang Y, Zhang W, Kong N, Zhang Q, Huang J (2014) Understanding the circulation of geothermal waters in the Tibetan Plateau using oxygen and hydrogen stable isotopes. *Appl. Geochem* 51:23–32
- Tong W, Zhang MT (1989) *Geothermal springs in Tengchong*. Science Press, Beijing (in Chinese)
- Truesdell AH, Fournier RO (1977) Procedure for estimating the temperature of a hot water component in a mixed water using a plot of dissolved silica vs. enthalpy. *US Geol. Surv. J. Res* 5: 49–52
- Truesdell AH, Hulston JR (2017) Hydrogeochemistry and genesis analysis of thermal and mineral springs in Arxan, Northeastern China. *Water* 9:61. <https://doi.org/10.3390/w9010061>
- Van Stempvoort DR, Krouse HR (1994) Controls of $\delta^{18}\text{O}$ in sulfate: review of experimental data and application to specific environments. pp. 446–480. DOI: <https://doi.org/10.1021/bk-1994-0550.ch029>
- Vonsée B, Crijns GW, Liu W (2019) Energy technology dependence—a value chain analysis of geothermal power in the EU. *Energy* 178: 419–435
- Wang GL, Zhang FW, Liu ZM (2000) An analysis of present situation and prospect of geothermal energy development and utilization in the world. *Acta Geoscientia Sinica* 21:124–137
- Wang ZL, Zhang J, Liu CQ (2007) Strontium isotopic compositions of dissolved and suspended loads from the main channel of the Yangtze River. *Chemosphere* 69(7):1081–1088. <https://doi.org/10.1016/j.chemosphere.2007.04.031>
- Wang YS, Chen JS, Chen L (2009) Tracing groundwater with strontium iso-topic compositions in the Hexi Corridor Basin, Northwestern China. *Adv. Water Resour. Hydraul. Eng.* 184–187 (in Chinese with English abstract)
- Wei WH, Ma R, Sun Z, Zhou A, Bu J, Long X, Liu Y (2018) Effects of mining activities on the release of heavy metals (HMs) in a typical mountain headwater region, the Qinghai-Tibet Plateau in China. *Int. J. Environ. Res. Public Health* 15:1987. <https://doi.org/10.3390/ijerph15091987>
- Zhao LJ, Yin L, Xiao HL, Cheng GD, Zhou MX, Yang YG, Li CZ, Zhou J (2011) Isotopic evidence for the moisture origin and composition

- of surface runoff in the headwaters of the Heihe River basin. Chinese Sci Bull 56, doi: <https://doi.org/10.1007/s11434-010-4278-x>
- Zhao RS, Shan XL, Yi J, Du XL, Liang Y, Zhang YF (2018) Geochemistry of HCO₃-Na thermal water from the Gudian slope: Insights into fluid origin, formation mechanism and circulation in the Yitong Basin, Northeast China. Appl. Geochem 91:185–196
- Zhou X, Li J, Zhou H, Fang B, Yu L, Li S (2008) Increase in thermal groundwater due to a flowing well near the Songshan hot spring in Beijing, China. Environ. Geol 53:1405–1411
- Zsolt AB, Doris S, Markus AL, Klinge H (2002) S- and O- isotopic character of dissolved sulphate in the cover rock aquifers of a Zechstein salt dome. Appl Geochem 17:1515–1528